Dynamical properties of the soft-wall elliptical billiard

Tiago Kroetz,[1,2] Hércules A. Oliveira,[3] Jefferson S. E. Portela,[1] and Ricardo L. Viana[2]

[1]*Departamento Acadêmico de Física, Universidade Tecnológica Federal do Paraná–UTFPR Campus Pato Branco, Pato Branco 85503-390, PR, Brazil*

[2]*Departamento de Física, Universidade Federal do Paraná–UFPR, Curitiba 81531-990, PR, Brazil*

[3]*Departamento Acadêmico de Matemática, Universidade Tecnológica Federal do Paraná–UTFPR Campus Ponta Grossa, Ponta Grossa 84016-210, PR, Brazil*

(Received 13 January 2016; revised manuscript received 27 June 2016; published 30 August 2016)

Physical systems such as optical traps and microwave cavities are realistically modeled by billiards with soft walls. In order to investigate the influence of the wall softness on the billiard dynamics, we study numerically a smooth two-dimensional potential well that has the elliptical (hard-wall) billiard as a limiting case. Considering two parameters, the eccentricity of the elliptical equipotential curves and the wall *hardness*, which defines the steepness of the well, we show that (1) whereas the hard-wall limit is integrable and thus completely regular, the soft wall elliptical billiard exhibits chaos, (2) the chaotic fraction of the phase space depends nonmonotonically on the hardness of the wall, and (3) the effect of the hardness on the dynamics depends strongly on the eccentricity of the billiard. We further show that the limaçon billiard can exhibit enhanced chaos induced by wall softness, which suggests that our findings generalize to quasi-integrable systems.

DOI: 10.1103/PhysRevE.94.022218

I. INTRODUCTION

A billiard is a system where a particle moves freely in a region enclosed by a boundary with which the particle suffers elastic collisions. The dynamics in such systems can be very rich and is completely determined by the geometry of the boundary [1]. Billiards have found several applications in physics, proving themselves particularly useful for the study of quantum chaos and its relation to classical nonlinear phenomena [2–9].

The elliptical billiard presents only regular motion, as constants of motion restrict the orbits to invariant curves in phase space [10–13]. These integrable orbits come in two types: the libration (always passing between the foci) and the rotation (never passing between the foci). The regions in phase space that contain each type of orbit are separated by the so-called separatrix.

This separation of two distinct kinds of motion motivated the study of the escape rates of an elliptical billiard with a hole placed on its boundary, considering billiards with both static and time-dependent walls [14]. The time-dependent elliptical billiard also permitted the investigation of Fermi acceleration, where particles can exhibit unlimited energy growth by impacting with the moving walls [15–20]. Since the dynamics in a static elliptical billiard is integrable, the existence of Fermi acceleration in the time-dependent elliptical billiard effectively extends the scope of the LRA Conjecture [21]. This conjecture states that static billiards presenting chaotic dynamics will display Fermi acceleration whenever their nonstatic counterpart boundaries have a periodic dependence with time. A separatrix is a homoclinic or an heteroclinic surface in phase space which is very sensitive to small perturbations and easily replaced by a stochastic layer due to a resonant interaction phenomena [22–24]. Due to this fact, even billiards with integrable dynamics but with a separatrix in phase space exhibit Fermi acceleration when a time dependence is imposed on the boundaries [25,26].

Besides time-dependent walls, another possible generalization of the concept of a billiard is that of a soft-wall system, where the Heaviside step potential that corresponds to the rigid wall of traditional, hard billiards is replaced by a smooth potential; i.e., the wall is *softened*. Soft billiard walls provide a more realistic model for trapped particles [27], since physically realizable potentials are typically smooth. Wall softness has so far been observed to have an stabilizing effect on the dynamics. For instance, the emergence of islands of stability from the tangent and corner periodic orbits of dispersing billiards as their walls become soft was shown by Rom-Kedar and Turaev [28–30]. Cold atoms confined in optical traps have been investigated numerical and experimentally [31–33], and soft walls were found to give rise to stable regions in phase space. These results corroborate previous theoretical results for dispersing chaotic billiards and also indicate they might generalize to focusing chaotic billiards. It has already been suggested that the softness of the wall could be a tunable parameter to control chaos [33], and, indeed, one could ask whether wall softness always enhances the stability of a system.

In this work we investigate a realization of the elliptical billiard with soft walls considering a two-dimensional smooth potential as a model [28,33–35]. We intend to determine the effect of softness on the dynamics of a billiard that is both integrable at the hard-wall limit and also presents a heteroclinic structure in phase space. We investigate the limaçon billiard as well, as an instance of a more general, nonintegrable system. We find that, similarly to the generalization of the LRA Conjecture, here too the phase space fragility seems to give rise to unexpectedly rich, unstable behavior, both in integrable and in quasi-integrable (hard-wall) billiards.

The paper is organized as follows. In Sec. II we present the elliptical billiard potential, its equations of motion, and typical trajectories. In Sec. III we define a Poincaré surface of section and investigate the transitions in the phase space as we vary the hardness of the billiard walls. In Sec. IV

we present the parameter space of the system and reveal its nontrivial order-chaos transitions. In Sec. V we consider a different billiard geometry, the limaçon, which also presents softness-induced chaos. Finally, we draw our conclusions and final considerations in Sec. VI.

II. SOFT-WALL BILLIARD

The motion of a particle in a soft-wall elliptical billiard is governed by the two-dimensional Hamiltonian

$$H = \frac{p_x^2}{2} + \frac{p_y^2}{2} + V(x,y), \tag{1}$$

where (x,y) is the particle position in rectangular coordinates, $p_{x,y}$ are the corresponding momenta, and the potential $V(x,y)$ defines the force exerted on the particle, i.e., the shape of the billiard. In order to obtain a tunable softness and the desirable geometry of the billiard, we choose

$$V(x,y) = \mathrm{erf}\left[h\left(x^2 + \frac{y^2}{b^2} - 1\right)\right], \tag{2}$$

where $\mathrm{erf}(z) = 2\pi^{-1/2}\int_0^z e^{-\tau^2}\,d\tau$ is the error function. The parameter h controls the hardness of the billiard: higher values correspond to steeper walls, and the equipotential curves are ellipses centered at the origin, with eccentricity $e = \sqrt{1-b^2}$. The potential V is null over an ellipse with semimajor axis equal to 1 and semiminor axis equal to b, and V is negative in the interior of this curve and positive outside. The hard-wall billiard is recovered as $h \mapsto \infty$, when $V \mapsto 1$ (-1) outside (inside) the null equipotential curve. The dependence of V on the hardness h is illustrated in Fig. 1.

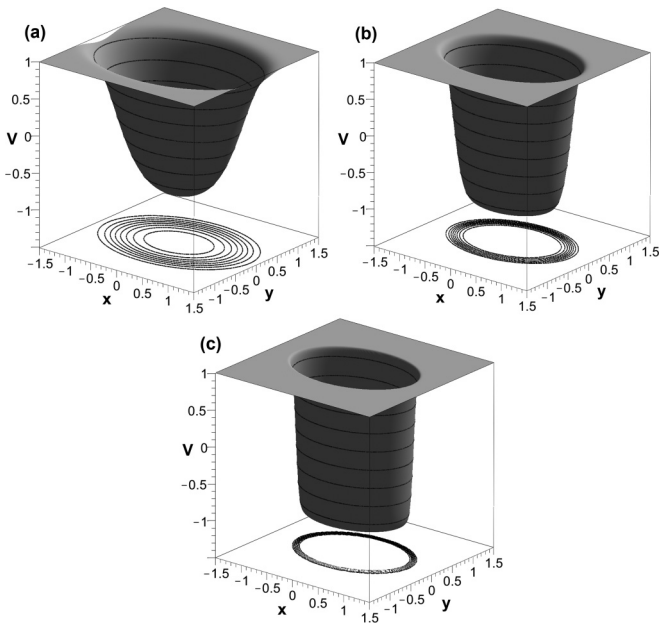

FIG. 1. Potential $V(x,y)$ for $e = 0.72$ and hardness (a) $h = 1$, (b) $h = 3$, and (c) $h = 8$.

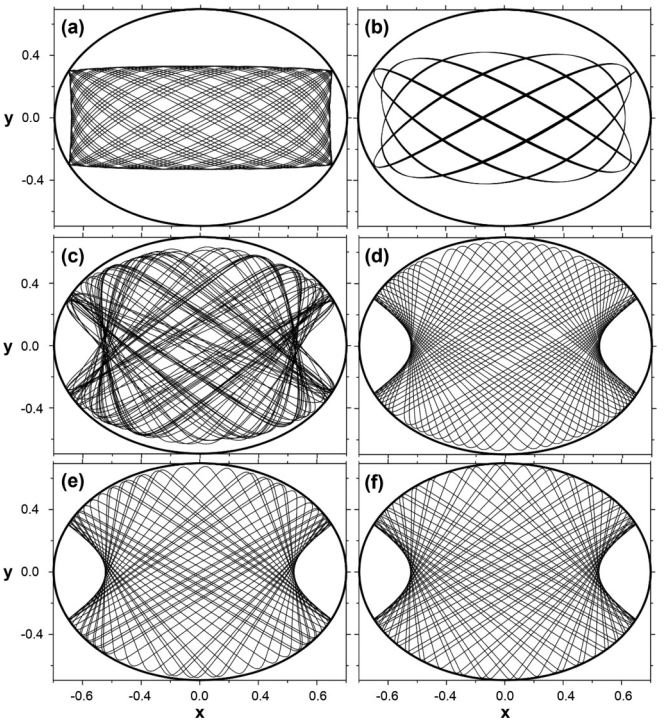

FIG. 2. Trajectories of energy $E = 0$ for the soft-wall elliptical billiard at several hardness values. The eccentricity is $e = 0.72$, and the initial condition is $(x,y) = (0.9,0.3025)$, $(p_x,p_y) = (0,0)$. The hardness is (a) $h = 0.5$, (b) $h = 1$, (c) $h = 2.5$, (d) $h = 6$, (e) $h = 8$, and (f) $h = 18$. Also displayed is the equipotential curve $V(x,y) = 0$, an absolute "wall" for the particles with the chosen energy.

The time evolution of the system is determined by Hamilton's equations:

$$\begin{aligned}
\frac{dx}{dt} &= \frac{\partial H}{\partial p_x} = p_x,\\
\frac{dp_x}{dt} &= -\frac{\partial H}{\partial x} = \frac{-4hx}{\sqrt{\pi}}\exp\left[-h^2\left(x^2 + \frac{y^2}{b^2} - 1\right)^2\right],\\
\frac{dy}{dt} &= \frac{\partial H}{\partial p_y} = p_y,\\
\frac{dp_y}{dt} &= -\frac{\partial H}{\partial y} = \frac{-4hy}{b^2\sqrt{\pi}}\exp\left[-h^2\left(x^2 + \frac{y^2}{b^2} - 1\right)^2\right],
\end{aligned} \tag{3}$$

which must be solved numerically. We use the Runge-Kutta method with adaptive step size dt and choose $dt = \epsilon_0 + \epsilon_1|V(x,y)|$, with $\epsilon_0 = 10^{-5}$ and $\epsilon_1 = 10^{-3}$, so that the step has an upper limit of order ϵ_1 and takes the smaller ϵ_0 value where the potential varies more abruptly, around $V(x,y) = 0$.

Typical trajectories lying on the energy surface $E = 0$ obtained from integrating Eq. (3) can be seen in Fig. 2 and Fig. 3, where the two different initial conditions considered for each figure correspond to a librator orbit and a rotator orbit, respectively, at the hard-wall limit. These figures show how the Lissajous-like orbits of the bow-shaped potential well change into the well-known regular orbits of the hard-wall elliptical billiard [10,14] as the hardness h increases. Remarkably,

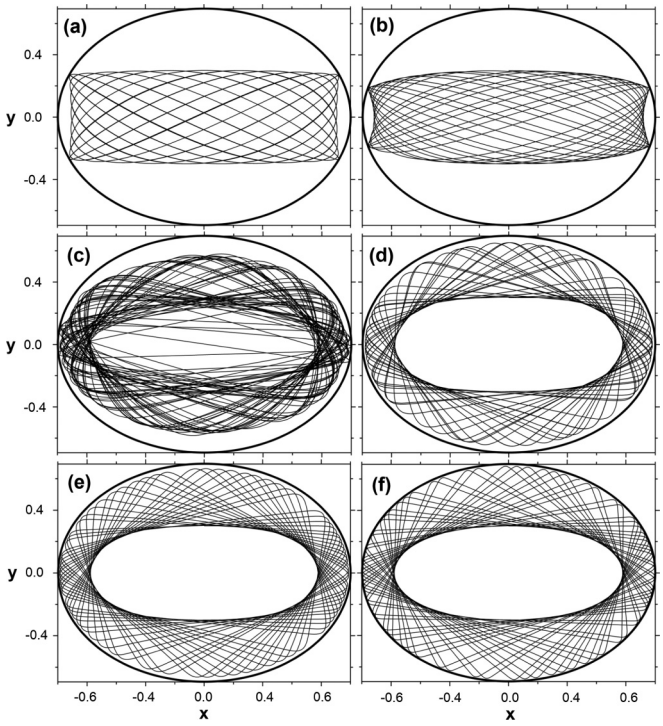

FIG. 3. The same as in Fig. 2, with the initial condition $(x,y) = (0,0.3)$, $p_y = 0$ and p_x determined by imposing $E = 0$. Hardness values are (a) $h = 0.5$, (b) $h = 1$, (c) $h = 2.5$, (d) $h = 6$, (e) $h = 8$, and (f) $h = 18$, with p_x varying between 0.932 and $\sqrt{2}$.

for $h = 2.5$, the system exhibits chaotic behavior [Figs. 2(c) and 3(c)].

III. POINCARÉ MAP

In conservative systems, the energy is an integral of motion that reduces the effective dimension of the system by one unity. Specifically, adopting polar coordinates (r,θ) centered at the bottom of the potential well to describe the particle position in the elliptical billiard, r, can be shown to be a dependent variable, given by

$$r = \sqrt{\frac{b^2}{b^2\cos^2\theta + \sin^2\theta}\left[\frac{h - \mathrm{erf}^{-1}(p^2/2 - E)}{h}\right]}. \qquad (4)$$

An additional dynamical variable can be eliminated from the system description by using a Poincaré surface of section [36], allowing us to describe the dynamics of the soft-wall elliptical billiard by means of a two-dimensional *map*. We devote Sec. III A to describing our surface of section and the map phase-space variables. The corresponding numerical results are in Sec. III B

A. Poincaré surface of section

Poincaré surfaces for hard-wall billiards are typically defined by reflections with the boundaries, while for smooth dynamical systems the surfaces are usually defined [37–39] by a condition such as $x = 0$. Although it would also be reasonable to define the Poincaré surface on $x = 0$ for the soft-wall elliptical billiard, displaying our results in a similar phase

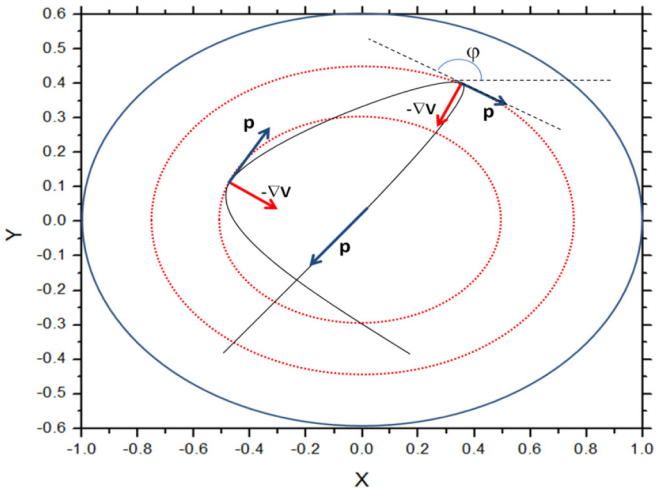

FIG. 4. Schematic representation of a trajectory traced by a particle in the soft-wall elliptical billiard. The trajectory crosses the Poincaré surface at each reflection at (tangency to) an equipotential curve. The angle with the horizontal direction of the equipotential curve at each reflection is φ.

space facilitates comparisons to the well-known properties of the hard-wall elliptical billiard. Therefore we need to define a Poincaré surface which is analogous to the reflections in hard-wall billiards. Reflections are characterized by reversal of the perpendicular component of the momentum relative to the wall, $p_\perp \mapsto -p_\perp$, a reversal that in soft-wall billiards happens when $p_\perp = 0$. Thus, we consider that a reflection takes place when the trajectory is tangent to an equipotential curve, as illustrated in Fig. 4. The condition for such a reflection can be written, from Eq. (3), as

$$\vec{p}\cdot\vec{F} = xp_x + \frac{y}{b^2}p_y = 0. \qquad (5)$$

We define the Poincaré surface as the plane $p_\perp = 0$, which is pierced by a trajectory when the condition above is satisfied, as the dot product changes signal from positive to negative. This corresponds to a reflected trajectory in configuration space (x,y) and to a point in the map phase space $(\theta, p_\parallel)$, where $p_\parallel$ is the component of the momentum parallel to the equipotential ellipse at the reflection and can be normalized with respect to its maximum value

$$p_{\max} = \sqrt{2[E + \mathrm{erf}(h)]}. \qquad (6)$$

In the coordinates used in the phase-space portraits, the Poincaré map is not symplectic, as $(\theta, p_\parallel)$ is not a canonically conjugated pair. Our numerical calculations, however, were performed in rectangular coordinates (x,y,p_x,p_y). The transformation between these variables at the reflection $(p_\perp = 0)$ is given by

$$x = r\cos\theta, \quad y = r\sin\theta,$$
$$p_x = p_\parallel\cos\varphi, \quad p_y = p_\parallel\sin\varphi, \qquad (7)$$

where φ is the angle between the equipotential (and therefore $p_\parallel$) and the horizontal direction, as illustrated in Fig. 4, and is

given by

$$\varphi = \tan^{-1}\left[\frac{-b'x}{a'^2\sqrt{1-x^2/a'^2}}\right], \tag{8}$$

where $b' = \sqrt{x^2(1-e^2)+y^2}$ and $a' = b'/\sqrt{(1-e^2)}$ are, respectively, the semiminor axis and the semimajor axis of the equipotential ellipse.

B. Influence of hardness on the dynamics

Much of the research on billiards aims to determine the influence of the control parameters on the dynamics of the system [40–43]. In this subsection, we focus on the transition between integrable and chaotic regimes in the soft-wall elliptical billiard as the hardness is varied. We begin this investigation by analyzing Poincaré plots for various values of hardness h. In each plot 160 initial conditions uniformly distributed over the phase space are integrated for 5000 reflections. We show in Fig. 5 some representative Poincaré plots for eccentricity $e = 0.72$ and energy $E = 0$. Empty regions at high $|p_\parallel|$ values indicate that the dynamics does not present reflections close to the direction tangent to the equipotential curves.

Some important features of the elliptical billiard with very soft, bowl-shaped walls [$h = 1$; see Fig. 1(a)] are revealed in Fig. 5(a): (1) absence of chaos; (2) absence of integrable spanning surfaces along θ direction in the phase space, i.e., rotator orbits as those observed in the hard-wall billiard; and (3) the stability of the orbit over the semimajor axis of the ellipse. The last mentioned orbit corresponds to the points $(\theta, p_\parallel) = (0,0)$ and $(\pi,0)$ in the Poincaré plot, which is unstable for the hard-wall case. The islands of quasiperiodicity around $(\theta, p_\parallel) = (0,0)$ and $(\pi,0)$ correspond to a set of librator orbits similar to those shown in Fig. 2(b).

It is possible to observe in Fig. 5(b) that by considering a higher value for the hardness parameter, $h = 1.7$, the trajectory over the semimajor axis rapidly loses its stability and bifurcates generating chaotic orbits close to the now unstable point. The two big islands remaining in phase space located around $(\theta, p_\parallel) = (\frac{\pi}{2},0)$ and $(\frac{3\pi}{2},0)$ correspond to the librator orbits close to the straight line trajectory over the semiminor axis, which are also stable for the hard-wall elliptical billiard. Increasing further the hardness, the area occupied by chaotic orbits in the phase space expands and constitutes a stochastic layer around the islands of librator orbits, as can be seen in Figs. 5(c) and 5(d).

Remarkably, the stochastic layer reverts its tendency of growth with h and starts to shrink at around $h = 6$. The integrable spanning curves at the top and at the bottom of Fig. 5(e), for $h = 6$, correspond to the rotator orbits around the two foci. In Fig. 5(f) it is possible to see that for an even higher hardness, for $h = 18$, the integrable spanning curves correspondent to the rotator orbits invade the stochastic layer, significantly reducing the presence of chaotic dynamics. At the limit $h \to \infty$, the hard-wall elliptical billiard is expected to be recovered. In this case, the stochastic layer must vanish and is replaced by a separatrix that segregates the only possible types of orbits in phase space: librations close the semiminor axis and rotations around the two foci.

This general scenario holds over a wide range of eccentricities. We illustrate this in Fig. 6, with Poincaré plots for the same

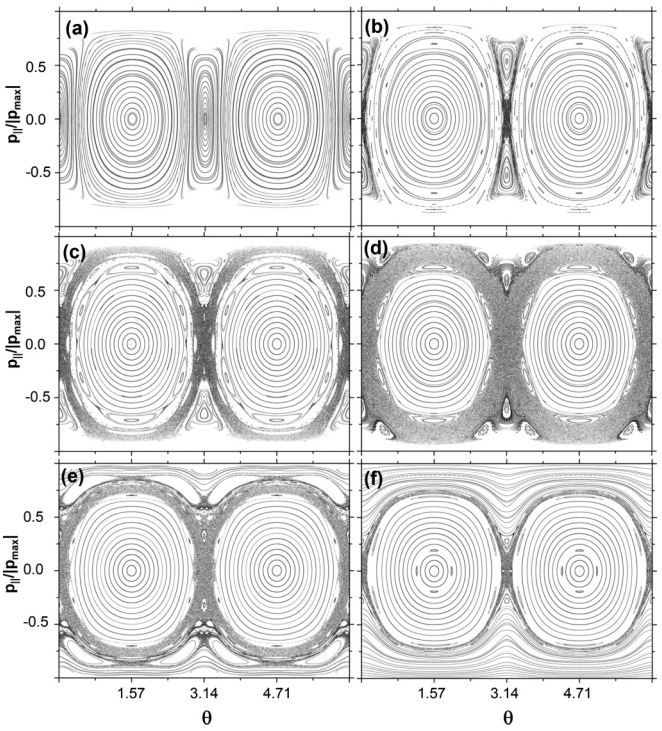

FIG. 5. Poincaré plots for the soft-wall elliptical billiard with eccentricity $e = 0.72$, energy $E = 0$, and hardness (a) $h = 1$, (b) $h = 1.7$, (c) $h = 2$, (d) $h = 2.5$, (e) $h = 6$, and (f) $h = 18$.

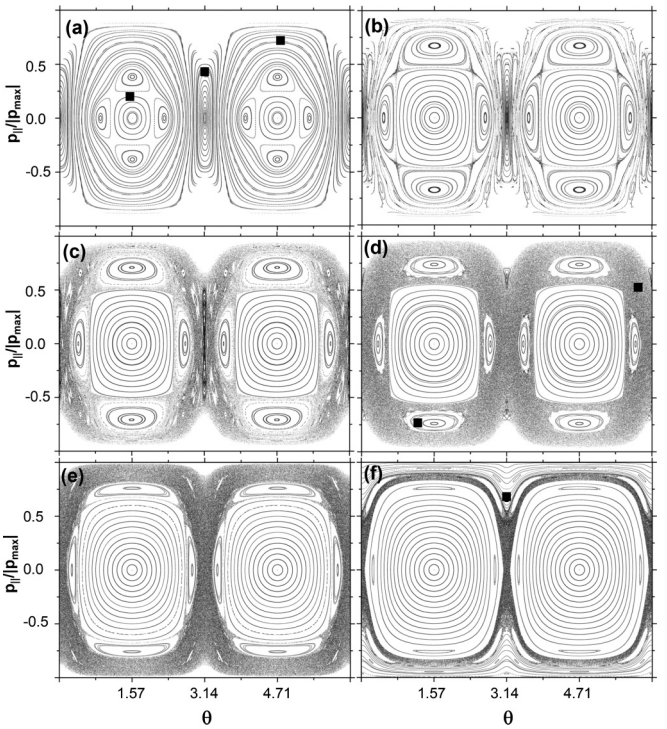

FIG. 6. Same as in Fig. 5, but with eccentricity $e = 0.84$. The squares indicate initial conditions for the trajectories shown in Fig. 7.

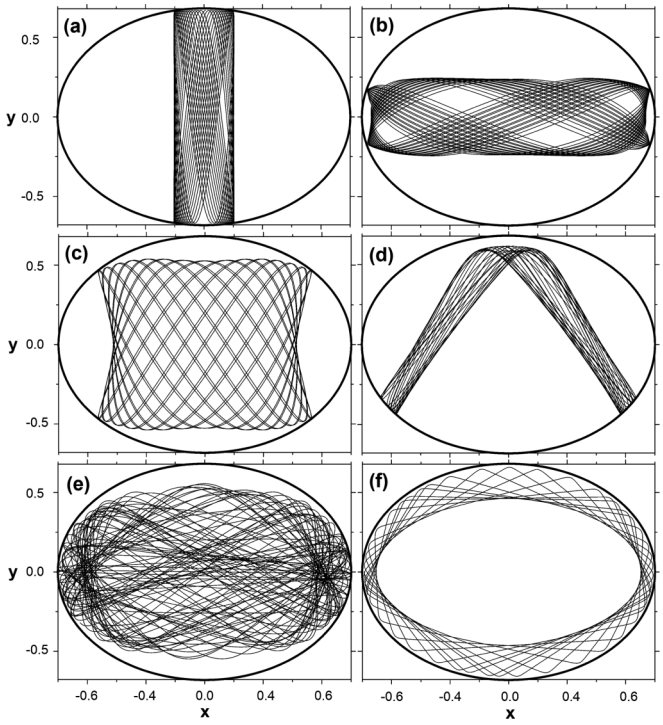

FIG. 7. Trajectories corresponding to different regions of the phase space plots shown in Fig. 6, where the trajectories initial conditions are also indicated. Trajectories in panels (a), (b), and (c) start, respectively, on the points marked by squares on the left side, on the center, and on the right side in Fig. 6(a). Trajectories in panels (d) and (e) correspond, respectively, to the squares on the left side and on the right side in Fig. 6(d); and panel (f) corresponds to the initial condition marked in Fig. 6(f).

values of parameter h and energy E as in Fig. 5, but for a higher eccentricity $e = 0.84$. Although we also observe an increase followed by a reduction of stochastic layer for $e = 0.84$, the area occupied by chaotic orbits is slightly greater when we compare Figs. 5(d) and 5(e) to Figs. 6(d) and 6(e).

The variety of behaviors exhibited by the soft-wall elliptical billiard is illustrated by the configuration space trajectories of Fig. 7, whose initial conditions are shown in the phase space portraits of Figs. 6(a), 6(d), and 6(f). The square on the left-side island in Fig. 6(a) originates the librator orbit close to the semiminor axis of Fig. 7(a). The initial condition marked by a square on the center island of the same figure leads to a librator orbit close to the semimajor axis of Fig. 7(b): a type of librator orbit that is possible only for low values of h. The larger libration orbit shown in Fig. 7(c) corresponds to the initial condition marked by the square on the outer curve of the island at the right side of Fig. 6(a). The distinctive trajectory of Fig. 7(d) corresponds to the initial condition marked by a square on the small island of Fig. 6(d). Such satellite islands persist with the changes in parameter h, and the corresponding trajectories are typical of soft-wall elliptical billiards. An initial condition in the stochastic layer, as indicated by the square on the right-hand side of Fig. 6(d), originates a clearly irregular orbit as shown in Fig. 7(e) and an initial condition over an integrable spanning curve, as that marked by the square in Fig. 6(f), results in the rotator orbit around two foci depicted in Fig. 7(f).

IV. PARAMETER SPACE

The Poincaré plots of Fig. 5 and of Fig. 6 paint the following picture of the billiard dynamics, as the hardness h is increased from zero: an initially regular dynamics experiences a break-up of integrability, and chaoticity reaches a maximum for a specific value of h followed by a gradual reduction of the chaotic sea in phase space, which asymptotically approaches to the hard-wall limit ($h \to \infty$) where the system becomes integrable again. This scenario also depends on the geometric parameter e, and, in this section, we investigate the two-dimensional parameter space (e,h) with respect to the fraction of phase space occupied by the chaotic sea, as well as to the largest Lyapunov exponent of the system.

The method used to estimate the occupation fraction is the box-counting analysis [44,45]. The phase space is divided in a grid, and the fraction of boxes that contain at least one point of a given orbit is a good approximation of the area this orbit fills. Regular orbits describe points or curves in the Poincaré phase space and have zero area. Chaotic orbits, on the other hand, belong to a chaotic sea of finite area. As a rule of thumb, the number of computed orbit points should be at least five times the number of boxes to ensure a good estimate [45]. We choose a 145×145 grid and evolve 51 initial conditions (one at the origin and the remaining randomly scattered) for 10^5 reflections, values we found to be sufficient to ensure numerical convergence. The occupation fraction related to each initial condition is thus obtained. The largest value for these fractions is our estimative for the size of the chaotic sea. Performing this calculation for a grid of (e,h) values, we obtain a detailed picture of the chaoticity of the billiard in its space of parameters.

We show in Fig. 8(a) the fraction of phase space occupied by the chaotic sea, as a function of the eccentricity and hardness, for orbits of energy $E = 0$. The chaoticity of the system displays a clearly nonmonotonic dependence on both parameters. We consider $e > 0.5$, since for lower eccentricities the system does not exhibit a relevant stochastic layer. Chaos is more prevalent for $2 < h < 5$ and $0.8 < e < 0.9$, reaching the largest value 51% of phase space occupation for $(e,h) \approx (0.84,2.5)$. For hardness $h \lesssim 2$ the billiard potential well approaches a harmonic-oscillator-like potential [$\mathrm{erf}(hz^2) \approx hz^2$ for small h] and regular behavior prevails. For $h \gtrsim 2$ chaos is always present, but as h is further increased the chaotic sea can be less or more persistent depending on the eccentricity, being, for example, more fragile for $e = 0.625$ and more robust for $e = 0.9$. The fish-bone-like fine structure is a result of high-order resonances taking place [46,47], with the corresponding satellite islands becoming alternately larger and smaller as the parameters are varied.

A remarkably similar picture is found for orbits of higher energy ($E = 0.7$, not shown), suggesting that the particle energy is not a decisive parameter for the elliptical billiard dynamics.

While the relative size of the chaotic sea measures the prevalence of chaos in the phase space, another important quantifier of chaoticity is the largest Lyapunov exponent,

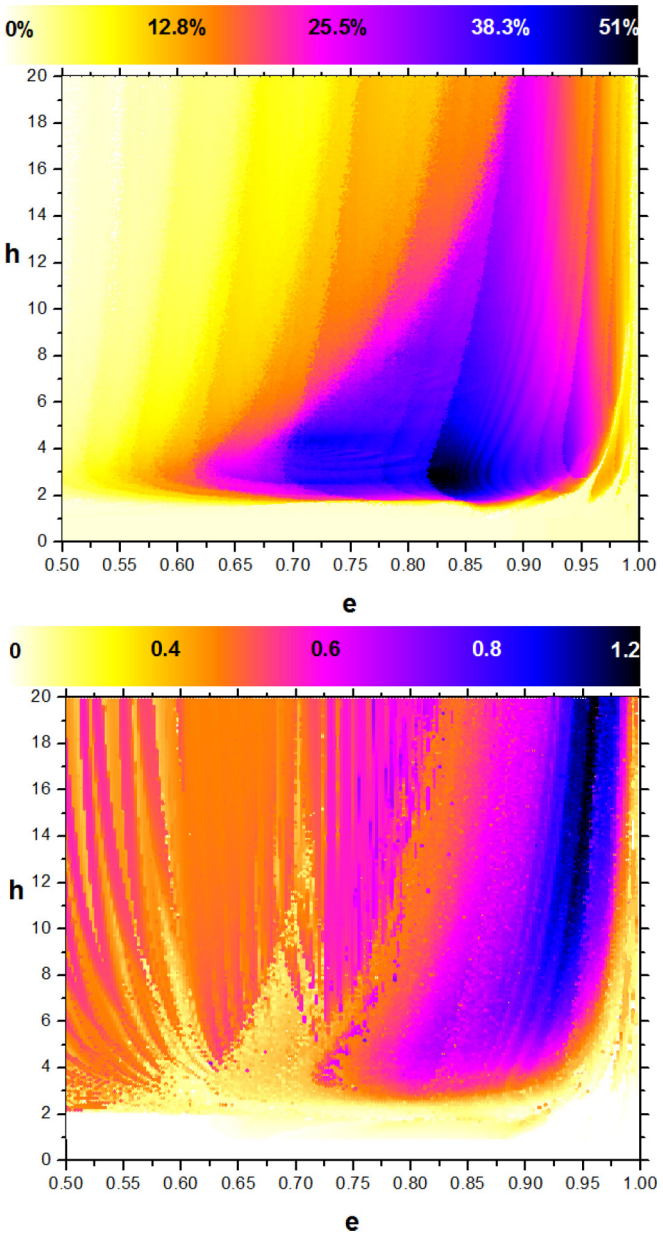

FIG. 8. Parameter space for the soft-wall elliptical billiard for orbits of energy $E = 0$. The scale indicates (a) the phase space fraction occupied by chaotic orbits and (b) the largest Lyapunov exponent.

which measures the chaos strength. The Lyapunov exponent is the average rate of exponential divergence of nearby orbits, and, following Wolf *et al.* [48,49], we evaluate the exponent by directly computing the divergence of probe orbits, for a range of parameter values. Our results for orbits of energy $E = 0$ in the soft-wall elliptical billiard are displayed in Fig. 8(b). A comparison between Figs. 8(a) and 8(b) reveals that, except for low chaoticity at very low hardness levels, there is little correlation between the two different measures, a result already known for billiards [44]. In particular, the decline of the stochastic layer size with increasing hardness is not accompanied by a decrease in sensitivity to initial conditions. Also, the largest chaotic seas and the strongest chaos do not occur in the same regions of the parameter space.

V. STOCHASTIC LAYER IN THE SOFT-WALL LIMAÇON BILLIARD

Our results for the soft-wall elliptical billiard indicate that softness-induced chaos arises in this system through the break-up of its separatrices. As the elliptical billiard is integrable in the hard-wall limit, it is enlightening to investigate how this mechanism plays out in a more general, nonintegrable billiard. The perturbative effect of smoothness should be evident, e.g., on the separatrix-like heteroclinic tangles KAM theory tells us enclose island chains in perturbed, quasi-integrable systems.

A simple perturbation of the (integrable) circular billiard is the one-parameter family of limaçon billiards introduced in Ref. [50], defined in polar coordinates by $r(\theta) = 1 + \epsilon \cos\theta$, where ϵ is the fractional deformation from the unit circle. The circular billiard is recovered for $\epsilon = 0$, and $\epsilon = 1$ results in the fully chaotic cardioid billiard [51].

As with the elliptical billiard, the soft-wall limaçon billiard can be described using the two-dimensional Hamiltonian H, Eq. (1), with the interaction between the particle and the billiard determined by the potential

$$V(x,y) = \mathrm{erf}\left[h\left(\sqrt{x^2+y^2} - \frac{\epsilon x}{\sqrt{x^2+y^2}} - 1\right)\right], \quad (9)$$

where h is the hardness parameter and the term inside the parentheses is the billiard boundary in rectangular coordinates. The potential of Eq. (9) is null over the boundary curve, negative in its interior and positive outside.

The time evolution of the system is determined by the Hamilton's equations, written now as

$$\begin{aligned}
\frac{dx}{dt} &= \frac{\partial H}{\partial p_x} = p_x, \\
\frac{dp_x}{dt} &= -\frac{\partial H}{\partial x} = \frac{-2h}{\sqrt{\pi}}\left[\frac{x-\epsilon}{\sqrt{x^2+y^2}} + \frac{\epsilon x^2}{(x^2+y^2)^{3/2}}\right] \\
&\quad \times \exp\left[-h^2\left(\sqrt{x^2+y^2} - \frac{\epsilon x}{\sqrt{x^2+y^2}} - 1\right)^2\right], \\
\frac{dy}{dt} &= \frac{\partial H}{\partial p_y} = p_y, \\
\frac{dp_y}{dt} &= \frac{\partial H}{\partial x} = \frac{-2h}{\sqrt{\pi}}\left[\frac{y}{\sqrt{x^2+y^2}} + \frac{\epsilon x y}{(x^2+y^2)^{3/2}}\right] \\
&\quad \times \exp\left[-h^2\left(\sqrt{x^2+y^2} - \frac{\epsilon x}{\sqrt{x^2+y^2}} - 1\right)^2\right], \quad (10)
\end{aligned}$$

which must solved numerically. We use the same Runge-Kutta method with adaptive step size described in Sec. II and the same Poincaré surface, defined by $p_\perp = 0$. This surface is

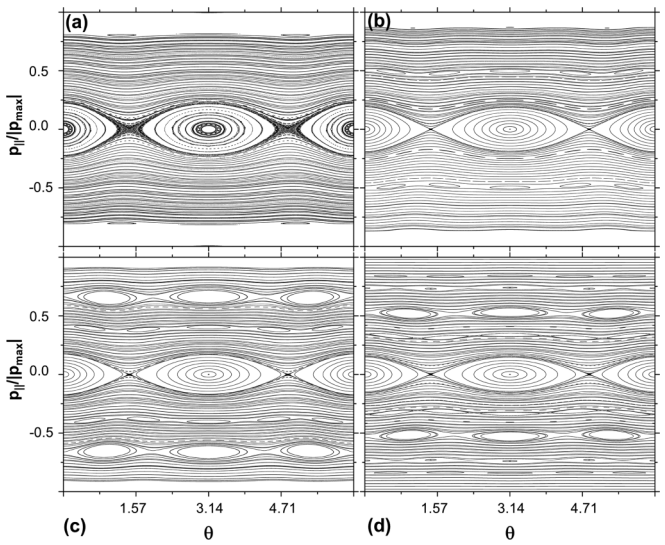

FIG. 9. Softness as a perturbing factor. Poincaré plots for the soft-wall limaçon billiard with fractional deformation $\epsilon = 0.15$, energy $E = 0$ and hardness (a) $h = 2.5$, (b) $h = 3.5$, (c) $h = 5$, and (d) $h = 20$.

pierced at the instants of reflections, when $\vec{p} \cdot \vec{F} = 0$, and hence the following relation is satisfied:

$$\frac{p_x}{\sqrt{x^2+y^2}}\left(x - \epsilon + \frac{\epsilon x^2}{x^2+y^2}\right) + \frac{p_y}{\sqrt{x^2+y^2}}\left(y + \frac{\epsilon xy}{x^2+y^2}\right) = 0. \quad (11)$$

The phase space for the lightly deformed limaçon billiard (Fig. 9) exhibits a stochastic layer for a low value of the hardness parameter h, i.e., as a result of the soft walls.

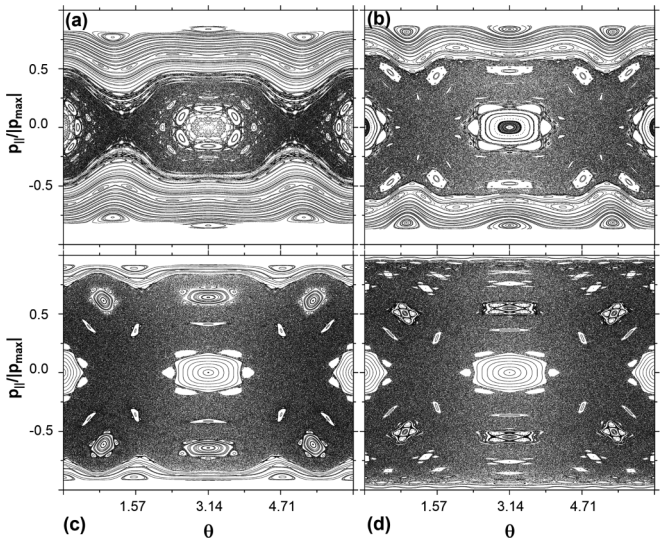

FIG. 10. Softness as a stabilizing factor. Poincaré plots for the soft-wall limaçon billiard with fractional deformation $\epsilon = 0.3$, energy $E = 0$, and hardness (a) $h = 2.5$, (b) $h = 3.5$, (c) $h = 5$, and (d) $h = 20$.

As the hardness is increased, the size of stochastic layer decreases abruptly and becomes restricted to a markedly thin area around the main island chain at the center of phase space.

The more strongly deformed limaçon billiard has a mixed phase space, with a sizable chaotic sea in the hard-wall limit [52]. For this case, the phase portraits of Fig. 10 reveal that softness has the opposite influence on the dynamics of that observed for the quasi-integrable situation (Fig. 9). As conjectured by Rom-Kedar and Turaev [28–30] and Kaplan *et al.* [31–33], the dynamics of the chaotic hard-wall billiard is stabilized by softness: as h increases, the regular tori spanning the top and bottom of the phase space are destroyed, giving place to an expanding chaotic sea.

VI. CONCLUSIONS

In order to investigate the dynamical properties of the soft-wall elliptical billiard, we introduce a Hamiltonian model consisting of a smooth two-dimensional potential well that has the hard-wall elliptical billiard as a limiting case. We also define a Poincaré surface of section using an analogue to the reflections with the hard walls, which allows a direct comparison of our results to the well-known properties of hard-wall elliptical billiard.

We find that the soft-wall elliptical billiard, in contrast to its integrable hard-wall counterpart, presents chaos for wide ranges of eccentricity and hardness. The soft-wall limaçon billiard with a low deformation replicates this observation, presenting increased chaoticity as hardness is decreased. This result complements the conclusions of Rom-Kedar and Turaev [28–30] and Kaplan *et al.* [31–33], who argue that the dynamics of hard-wall billiards turns more regular when softness (inverse of hardness) is incorporated into the model: The softness introduces resonances to the system, and, while Rom-Kedar and Turaev show that these resonances lead to the appearance of islands in phase space which reduce the size of the chaotic sea, we have shown that these resonances can also destroy the heteroclinic structure that constitutes a separatrix, giving rise to a stochastic layer which can grow into a chaotic sea.

In the elliptical billiard, this stochastic layer expands as the potential becomes softer (h is reduced) and reaches a maximum. As we continue to reduce the hardness of the walls, the system recovers stability through a bifurcation cascade that culminates with the separatrix heteroclinic orbit at the origin, and its associated stochastic layer, being replaced by an island. We found the effect of h on the chaotic sea to depend nontrivially on the eccentricity e of the potential. The interplay of both quantities, h and e, results in a rich parameter space structure which remain to be fully explored.

ACKNOWLEDGMENT

This work was made possible through the financial support from the Brazilian research agencies CNPq and Fundação Araucária.

[1] N. Chernov and R. Markarian, *Chaotic Billiards*, Mathematical Surveys and Monographs 127 (American Mathematical Society, Providence, RI, 2006).
[2] E. G. Altmann, J. S. E. Portela, and T. Tél, Rev. Mod. Phys. **85**, 869 (2013).
[3] M. V. Berry, J. Phys. A: Math Gen. **35**, 3025 (2002).
[4] H.-J. Stöckmann and J. Stein, Phys. Rev. Lett. **64**, 2215 (1990).
[5] L. A. Ponomarenko, F. Schedin, M. I. Katsnelson, R. Yang, E. W. Hill, K. S. Novoselov, and A. K. Geim, Science **320**, 356 (2008).
[6] M. Hentschel and K. Richter, Phys. Rev. E **66**, 056207 (2002).
[7] O. Bohigas, M. J. Giannoni, and C. Schmit, Phys. Rev. Lett. **52**, 1 (1984).
[8] B. Dietz and A. Richter, Chaos **25**, 097601 (2015).
[9] S. K. Joseph, J. Sabuco, L. Y. Chew, and M. A. F. Sanjuán, Opt. Express **23**, 32191 (2015).
[10] M. V. Berry, Eur. J. Phys. **2**, 91 (1981).
[11] A. Delshams, Y. Fedorov, and R. Ramírez-Ros, Nonlinearity **14**, 1141 (2001).
[12] V. Dragović, B. Jovanović, and M. Radnović, J. Geom. Phys. **47**, 221 (2003).
[13] V. Dragović and M. Radnović, Russ. Math. Surveys **65**, 319 (2010).
[14] F. Lenz, F. K. Diakonos, and P. Schmelcher, Phys. Rev. E **76**, 066213 (2007).
[15] E. D. Leonel and L. A. Bunimovich, Phys. Rev. Lett. **104**, 224101 (2010).
[16] F. Lenz, F. K. Diakonos, and P. Schmelcher, Phys. Rev. Lett. **100**, 014103 (2008).
[17] F. Lenz, C. Petri, F. R. N. Koch, and F. K. Diakonos, New J. Phys. **11**, 083035 (2009).
[18] D. F. M. Oliveira and M. Robnik, Int. J. Bifurcat. Chaos **22**, 1250207 (2012).
[19] A. L. P. Livorati, T. Kroetz, C. P. Dettmann, I. L. Caldas, and E. D. Leonel, Phys. Rev. E **86**, 036203 (2012).
[20] T. Kroetz, A. L. P. Livorati, E. D. Leonel, and I. L. Caldas, Phys. Rev. E **92**, 012905 (2015).
[21] A. Loskutov, A. R. Ryabov, and L. G. Akinshin, J. Phys. A: Math. Gen. **33**, 7973 (2000).
[22] A. C. J. Luo and R. P. S. Han, Chaos, Solitons Fractals **12**, 2493 (2001).
[23] S. S. Abdullaev, Phys. Rev. E **70**, 046202 (2004).
[24] A. Delshams and R. Ramírez-Ros, Nonlinearity **9**, 1 (1996).
[25] V. Gelfreich and D. Turaev, J. Phys. A: Math. Theor. **41**, 212003 (2008).
[26] V. Gelfreich, V. Rom-Kedar, and D. Turaev, Chaos **22**, 033116 (2012).
[27] Y.-U. Kim, U. Kuhl, H-J. Stöckmann, and J. P. Bird, J. Phys.: Condens. Matter **17**, L191 (2005).
[28] D. Turaev and V. Rom-Kedar, Nonlinearity **11**, 575 (1998).
[29] V. Rom-Kedar and D. Turaev, Chaos **22**, 026102 (2012).
[30] V. Rom-Kedar and D. Turaev, Phys. D **130**, 187 (1999).
[31] N. Friedman, A. Kaplan, D. Carasso, and N. Davidson, Phys. Rev. Lett. **86**, 1518 (2001).
[32] A. Kaplan, N. Friedman, M. Andersen, and N. Davidson, Phys. Rev. Lett. **87**, 274101 (2001).
[33] A. Kaplan, N. Friedman, M. Andersen, and N. Davidson, Phys. D: Nonlinear Phenom. **187**, 136 (2004).
[34] R. Ketzmerick, Phys. Rev. B **54**, 10841 (1996).
[35] H. A. Oliveira, C. Manchein, and M. W. Beims, Phys. Rev. E **78**, 046208 (2008).
[36] M. Tabor, *Chaos and Integrability in Nonlinear Dynamics: An Introduction* (Wiley-Interscience, New York, 1989).
[37] M. Hénon and C. Heiles, Astron. J. **69**, 73 (1964).
[38] G. Contopoulos, Z. Astrophysik **49**, 273 (1960).
[39] B. Barbanis, Astron. J. **71**, 415 (1966).
[40] D. F. M. Oliveira and E. D. Leonel, Commun. Nonlinear Sci. Numer. Simulat. **15**, 1092 (2010).
[41] A. L. P. Livorati, A. Loskutov, and E. D. Leonel, J. Phys. A: Math. Theor. **44**, 175102 (2011).
[42] P. Bálint, M. Halász, J. A. Hernández-Tahuilán, and D. P. Sanders, Nonlinearity **24**, 1499 (2011).
[43] J. Chen, L. Mohr, H.-K. Zhang, and P. Zhang, Chaos **23**, 043137 (2013).
[44] H. R. Dullin, P. H. Richter, and A. Wittek, Chaos **6**, 43 (1996).
[45] V. Lopac and A. Šimić, Commun. Nonlinear Sci. Numer. Simullat. **16**, 309 (2011).
[46] L. Reichl, *The Transition to Chaos: Conservative Classical Systems and Quantum Manifestations* (Springer-Verlag, New York, 2004).
[47] E. Ott, *Chaos in Dynamical Systems* (Cambridge University Press, Cambridge, 2002).
[48] A. Wolf, J. B. Swift, H. L. Swinney, and J. A. Vasano, Phys. D **16**, 285 (1985).
[49] J. C. Sprott, *Chaos and Time-Series Analysis* (Oxford University Press, Oxford, 2003).
[50] M. Robnik, J. Phys. A: Math. Gen. **16**, 3971 (1983).
[51] H. R. Dullin and A. Bäcker, Nonlinearity **14**, 1673 (2001).
[52] A. Bäcker and R. Schubert, J. Phys. A: Math. Gen. **35**, 527 (2002).